Dielectric and Pyroelectric Properties of Ammonium Hydrogen-DL-Malate Monohydrate, $NH_4(C_4H_5O_5) \cdot H_2O$

Silvia Fleck*, Michael C. Böhm, and Alarich Weiss

Institut für Physikalische Chemie, Physikalische Chemie III, Technische Hochschule Darmstadt, Darmstadt

Z. Naturforsch. **42 a**, 57–66 (1987); received August 13, 1986

The dielectric and pyroelectric properties of ammonium hydrogen-DL-malate monohydrate $NH_4^{\oplus}(^{\ominus}OOCCHOHCH_2COOH) \cdot H_2O$ were studied as a function of temperature and crystallographic direction. The components of the dielectric tensor at room temperature are within the limits $5.9 \leqq \varepsilon \leqq 8.6$. The pyroelectric coefficient $|\boldsymbol{p}|$ increases from $\approx 18\,\mu C\,m^{-2}\,K^{-1}$ at $T = 100$ K to $32\,\mu C\,m^{-2}\,K^{-1}$ at room temperature. The angular variation of $\boldsymbol{p}$ in the ac-plane of the crystal with symmetry Cc is $\approx 10°$.

Using an INDO procedure which includes crystal field effects in a self-consistent way (SCEF) the charge distribution in the solid was calculated. With the therefrom resulting dipole moment and together with the dielectric measurements the pyroelectric coefficient $|\boldsymbol{p}|$ and the change of $|\boldsymbol{p}|$ with temperature was calculated. Experiment and theoretical result agree satisfactory.

Introduction

Ammonium hydrogen-DL-malate monohydrate, $NH_4^{\oplus}(^{\ominus}OOCCHOHCH_2COOH) \cdot H_2O$, (AMAL) crystallizes in the monoclinic space group C_s^4-Cc [1] with only one symmetry element, a glide plane. In contrast, ammonium hydrogen L-malate, $NH_4^{\oplus}(^{\ominus}OOCCHOHCH_2COOH)$, crystallizes in the orthorhombic space group D_2^4-$P2_12_12_1$ [2, 3]. The two structures are substantially different, e.g. even the geometrical parameters of the malate ion differ in important details.

The lacking center of symmetry in the title compound is responsible for its interesting physical properties like optical anisotropy. Betzler et al. [4] have shown that AMAL can be used for phase-matched second harmonic generation. Other physical properties, which can be observed in the monoclinic domatic space group are piezoelectricity and pyroelectricity. For crystals with the space group Cc the problem arises that the spontaneous polarization can have any direction within the symmetry plane, in contrast to symmetry classes with a unique polar axis which fixes the direction of the spontaneous polarization. A well studied substance with the space group Pm is for example the ferroelectric compound lithium trihydrogen selenite, $LiH_3(SeO_3)$, and its deuterated analogue [5, 6]. In the following we report an investigation of the pyroelectric coefficient and the dielectric constant of AMAL and its temperature dependence.

Reprint requests to Prof. Dr. Al. Weiss, Institut für Physikalische Chemie III, Petersenstraße 20, D-6100 Darmstadt, West-Germany.

* Part of the Dr.-Ing. Dissertation S. Fleck, Darmstadt.

Experimental

Preparation

Ammonium hydrogen-DL-malate monohydrate was prepared from commercial components in stoichiometric amounts (DL-malic acid and ammonium hydroxide). The composition of the crystals was determined by chemical analysis (calculated values in brackets): C: 28.12% (28.41%), H: 6.53% (6.56%), and N: 8.32% (8.28%).

Large single crystals, $30 \times 20 \times 15\ mm^3$, can be grown by slow cooling of a seeded aqueous solution from $T = 305$ K to 295 K. Identification of the crystal axes and faces was made by comparison of the optical measurements with the crystal structure data [1]. The habitus of the crystal is shown in Figure 1.

For the measurement of the dielectric constant $\varepsilon = \varepsilon' - i\,\varepsilon''$ and the pyroelectric coefficient $\boldsymbol{p}$, different oriented crystal plates were cut in slices with a wire saw. The actual orientation of the crystal has been checked by optical measurements.

0340-4811 / 87 / 0100-0057 $ 01.30/0. – Please order a reprint rather than making your own copy.

Dieses Werk wurde im Jahr 2013 vom Verlag Zeitschrift für Naturforschung in Zusammenarbeit mit der Max-Planck-Gesellschaft zur Förderung der Wissenschaften e.V. digitalisiert und unter folgender Lizenz veröffentlicht: Creative Commons Namensnennung-Keine Bearbeitung 3.0 Deutschland Lizenz.

This work has been digitalized and published in 2013 by Verlag Zeitschrift für Naturforschung in cooperation with the Max Planck Society for the Advancement of Science under a Creative Commons Attribution-NoDerivs 3.0 Germany License.

Zum 01.01.2015 ist eine Anpassung der Lizenzbedingungen (Entfall der Creative Commons Lizenzbedingung „Keine Bearbeitung") beabsichtigt, um eine Nachnutzung auch im Rahmen zukünftiger wissenschaftlicher Nutzungsformen zu ermöglichen.

On 01.01.2015 it is planned to change the License Conditions (the removal of the Creative Commons License condition "no derivative works"). This is to allow reuse in the area of future scientific usage.

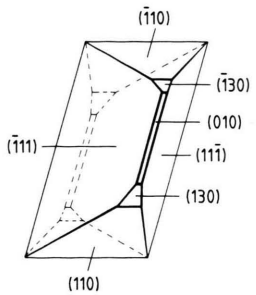

Fig. 1. Habitus of ammonium hydrogen-DL-malate monohydrate, $NH_4^{\oplus}(^{\ominus}OOCCHOHCH_2COOH) \cdot H_2O$.

The two opposite faces of the crystal plates were polished and painted with air drying silver paste. By this method single crystal capacitors with an area $15 \leqq A/mm^2 \leqq 60$, thickness $0.4 \leqq d/mm \leqq 0.8$ and filled with a single crystal dielectricum were obtained.

Measurement of the Dielectric Constants and the Pyroelectric Coefficient

The impedance of the different oriented single crystal capacitors was measured in a temperature range from 200 K to the decomposition temperature, T_d, using the bridge method described in [7]. The measurement of the actual temperature at the sample site was accurate to $\pm$ 0.5 K and the dielectric measurements were limited in accuracy by the determination of the crystal area and its thickness to 3%. Only $\varepsilon = \varepsilon'$ is given in the following. ε'' is very small and values $\varepsilon'' > 0.1$ are found near T_d.

The pyroelectric coefficient $\boldsymbol{p}$ at constant stress was measured on different oriented single crystal capacitors in the temperature range $100 \leqq T/K \leqq T_d$. As earlier [7, 8], the method of constant temperature variation was used, employing a temperature variation rate of $0.5 \leqq T \cdot t^{-1}/(K\,min^{-1}) \leqq 2$. For each crystal direction investigated, the measurements of ε and $\boldsymbol{p}$ were repeated using different plates. An accuracy for the pyroelectric coefficient of $\pm$ 8% was achieved.

In the range $245 \leqq T/K \leqq T_d$ the pyroelectric voltage was also measured with the low frequency sinusoidal temperature oscillation method. The temperature oscillations were created by a Peltier element with a frequency of 0.01 Hz and temperature amplitudes of $0.5 \leqq T/K \leqq 3$ [7, 8]. The accuracy of the temperature determination was in this case $\pm$ 0.3 K, and that of the pyroelectric coefficient was $\pm$ 5%.

Calculation of Dipole Moments in Solids

In order to discuss the temperature dependence of the pyroelectric coefficient in terms of molecular properties, it is necessary, to calculate the dipole moment of AMAL. This was done by two methods. At first, the dipole moment $\boldsymbol{\mu}$ was determined using dipole moment increments for each bond or group [9, 10] and the known value of $\boldsymbol{\mu}$ for H_2O [11], respectively. There are some uncertainties in this method. For example, the dipole moment for the group $-C\lessdot^{O}_{OH}$ found by summing up the values of the bond increments given in literature [10] differs appreciably from the dipole moment increment reported for this group. Also the variation of the dipole moment of the C–H bonds due to the neighbouring groups is not included in the increment method. Furthermore, to calculate the total resulting dipole moment on the basis of the method of increments, the partial dipole moment has to be found which results from the charge separation between the $NH_4^{\oplus}$ ion and the group $(-C\lessdot^{O}_{O})^{\ominus}$.

The data gained from the empirical increment method are somewhat arbitrary and not satisfactory. The solid state effect is completely neglected.

Calculation of the Dipole Moment by Semiempirical Methods of Quantum Chemistry

The basis for a theoretical determination of electric dipole moments in solids is the calculation of charge distributions. We have studied the electronic structure of AMAL on the basis of a semiempirical LCAO MO model of the INDO-type (intermediate neglect of differential overlap) [12], using an improved modification [13]. Solid state effects have been simulated by means of a self-consistent electrostatic field (SCEF) approach [14, 15] which leads to an approximative expression for the interaction energy between a preselected reference molecule and its neighbours. Dispersion energies and exchange interactions are neglected in the present SCEF formalism [16]. The perturbational approach is thus suitable for the investigation of intermolec-

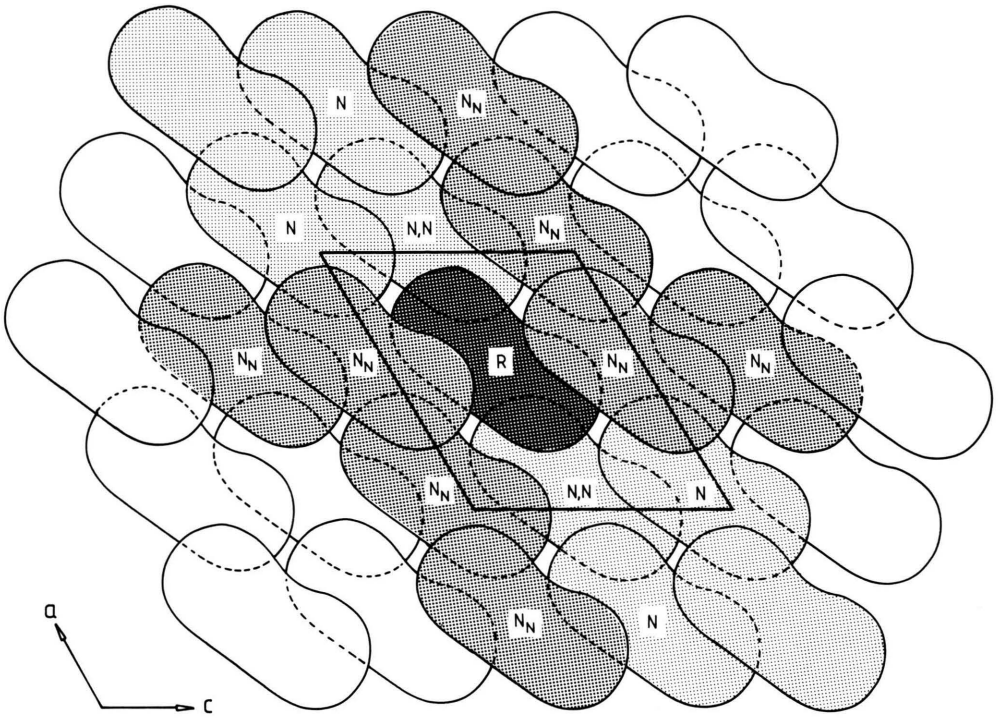

Fig. 2. Schematic display of the molecular arrangement of AMAL. The darkest area symbolizes the reference molecule R. In two different approximations the electron distribution in R is determined a) under the influence of the electrostatic field created by the nearest neighbours N_N (dark grey areas) and b) from the electrostatic field due to all neighbours N_N and N (given by the dark and light grey areas).

ular interactions that are largely determined by electrostatic (Coulomb) terms while covalency effects due to the kinetic energy of the electrons are small in comparison to the former interaction potential. This condition should be fullfilled in the title compound where the solid state arrangement is built up via hydrogen bonds between adjacent molecular units; the atomic centers forming the hydrogen bonds show always large charge separations.

The basis of the employed model is the fragmentation of the total solid into a reference molecule (R), whose electronic structure is treated explicitely, and environment molecules (N). The coupling between both units is handled in the frame of the mean field approximation. The partitioning scheme is sketched in Figure 2. The corresponding mean field operator $\hat{F}$ is given by an operator $\hat{F}_0$ associated to a single molecular unit and by the operator $\hat{F}_{ef}$, which describes an electrostatic coupling between the reference molecule and the environment,

$$\hat{F} = \hat{F}_0 + \hat{F}_{ef}. \tag{1}$$

For the numerical approach it is necessary to take into account the coupling between the reference unit R and the external ones N; the coupling between external units is thereby neglected:

$$\hat{H}_{RN} \neq 0; \quad \hat{H}_{NN'} = 0. \tag{2}$$

The perturbational Hamiltonian $\hat{H}_{ef}$ is defined by

$$\hat{H}_{ef} = \sum_{\mu=1}^{n} \sum_{N} \left(\sum_{j} \frac{Z_j}{\boldsymbol{r}_{\mu j}} - \sum_{j} \sum_{\nu=1}^{n} B_{\nu\nu} \int \frac{\nu(2) \cdot \nu(2)}{\boldsymbol{r}_{\mu\nu}} \, \mathrm{d}\tau \right). \tag{3}$$

The first term in (3) corresponds to the core contribution from the external field, the second one to the two electron part of $\hat{H}_{ef}$, with

μ = μ-th AO in the reference unit,
Z_j = atomic core charge of the j-th atom in the N-th external unit,
$\boldsymbol{r}_{\mu j}$ = distance vector between j-th atom in N-th external unit and μ-th AO in R,
$\boldsymbol{r}_{\mu\nu}$ = distance between the ν-th AO in N and the μ-th AO in R,
$B_{\nu\nu}$ = is the ν-th diagonal element of the bond order matrix.

By means of a simple central field monopole approximation it is possible to reduce $\hat{H}_{ef}$ to an operator of the one-electron type [17, 18]

$$\hat{H}_{ef} = \sum_{\mu=1}^{n} \sum_{N} \sum_{j} \frac{q_j}{r_{\mu j}} \tag{4}$$

with q_j = atomic net charge of the j-th centre in the N-th neighbouring unit. The matrix elements of the perturbational Fock operator are defined below: diagonal terms are given in (5) and the off-diagonal terms in (6). The off-diagonal elements are found by means of the Mulliken approximation [19]

$$F_{\mu\mu,\,ef} = \sum_{N} \sum_{j} q_j V_{\mu j}\,, \tag{5}$$

$$F_{\mu\nu,\,ef} = \tfrac{1}{2} S_{\mu\nu}(F_{\mu\mu,\,ef} + F_{\nu\nu,\,ef})\,, \tag{6}$$

with $V_{\mu j}$ = electron core interaction and $S_{\mu\nu}$ = overlap integral.

The equations show the necessary computational steps. i) A trial collection of atomic net charges q_j is determined for the isolated molecule. These q_j numbers are used to construct the external field. ii) Diagonalization of the complete Hartree-Fock operator leads to a new collection of q_j numbers, which are iterated up to SCEF convergence $\Delta E = 10^{-4}$ a.u.

Results

Dielectric Constant

Ammonium hydrogen-DL-malate monohydrate crystallizes with the space group Cc and the dielectric tensor has the form: (ε_{ij}); $i,j = 1, 2, 3$; $\varepsilon_{ij} = \varepsilon_{ji}$; $\varepsilon_{12}, \varepsilon_{23} = 0$. ε_{22} is obtained directly from measurements of the dielectric constant on a (010)-crystal plate (curve IV in Figure 3). The other components of the dielectric tensor, $\varepsilon_{11}, \varepsilon_{13}, \varepsilon_{33}$, describe an ellipse in the ac-plane of the crystal. They can be calculated from measurements of the dielectric constant in more than three directions within the (010)-plane by a formalism given by Nye [20]; the principles of this method are summarized below. If A_i is the value of the dielectric constant in the selected direction characterized by θ, θ = angle between the selected direction and the [100]-axis, A_i is given by

$$A_i = (\sin\theta_i \quad 0 \quad \cos\theta_i) \begin{pmatrix} \varepsilon_{11} & 0 & \varepsilon_{13} \\ 0 & \varepsilon_{22} & 0 \\ \varepsilon_{13} & 0 & \varepsilon_{33} \end{pmatrix} \begin{pmatrix} \sin\theta_i \\ 0 \\ \cos\theta_i \end{pmatrix}$$

$$= \sin^2\theta_i \cdot \varepsilon_{11} + \sin 2\theta_i \cdot \varepsilon_{13} + \cos^2\theta_i \cdot \varepsilon_{33}\,. \tag{7}$$

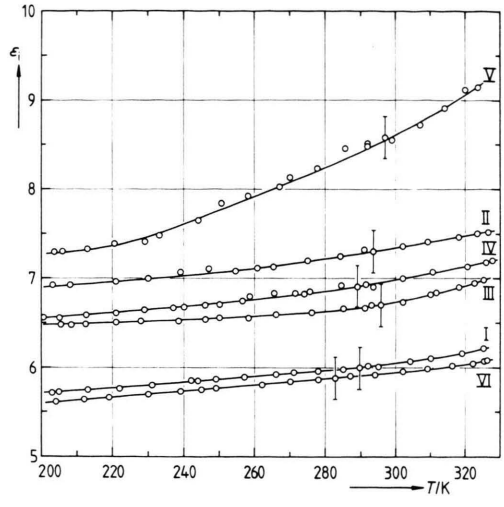

Fig. 3. Components of the dielectric constant in the ac-plane characterized by θ = angle between the direction of measurement and a preferred crystallographic vector. I–V: θ_i = angle between the direction of $\varepsilon_{I,\ldots,V}$ and the axis [100]. I) $\theta_I = 142.1°$; here the direction of the measurement corresponds to the normal of the plane $(10\bar{1})$. II) $\theta_{II} = 52.1°$. III) $\theta_{III} = 30.6°$; here the direction of measurement corresponds to the normal of the plane (100). IV) $\theta_{IV} = 120.6°$. V) $\theta_V = 90°$; this direction corresponds to the normal of the plane (001). θ_{VI} corresponds to the measurement on a plate cut parallel to the plane (010).

For AMAL A_i was measured in five different directions θ_i, $i = I \ldots V$ (see Fig. 3) and a set of similar equations is obtained.

$$A = \theta \cdot \varepsilon\,; \tag{8}$$

with

$$A = \begin{pmatrix} A_I \\ \vdots \\ A_V \end{pmatrix}, \quad \theta = \begin{pmatrix} \sin^2\theta_I & \sin 2\theta_I & \cos^2\theta_I \\ \vdots & \vdots & \vdots \\ \sin^2\theta_V & \sin 2\theta_V & \cos^2\theta_V \end{pmatrix}, \quad \varepsilon = \begin{pmatrix} \varepsilon_{11} \\ \varepsilon_{13} \\ \varepsilon_{33} \end{pmatrix}.$$

ε can be calculated by solving the equation

$$\varepsilon = (\theta_t\,\theta)^{-1}\,\theta_t \cdot A\,. \tag{9}$$

The tensor of the dielectric constant obtained for $T = 200$ K and $T = 300$ K in the crystallophysical system a, b, z, with z perpendicular to a and b, reads

$$\varepsilon(200\text{ K}) = \begin{pmatrix} 5.57 & 0 & 0.41 \\ 0 & 5.60 & 0 \\ 0.41 & 0 & 7.26 \end{pmatrix},$$

$$\varepsilon(300\text{ K}) = \begin{pmatrix} 5.35 & 0 & 0.47 \\ 0 & 5.95 & 0 \\ 0.47 & 0 & 8.34 \end{pmatrix}.$$

Using the circle construction of Mohr [20] the angle Φ between the principle axis of the ellipse and the axis [100] can be found. The experiment gave $\Phi = 77°$ and $81.3°$ for $T = 200$ K and $T = 300$ K, respectively. Therefrom the dielectric tensor in the principal coordinate system is

$\varepsilon(200\text{ K})$: $\varepsilon_{11} = 5.55$; $\varepsilon_{22} = 5.60$; $\varepsilon_{33} = 7.29$;

$\varepsilon(300\text{ K})$: $\varepsilon_{11} = 5.34$; $\varepsilon_{22} = 5.95$; $\varepsilon_{33} = 8.36$.

The Pyroelectric Coefficient

AMAL belongs to the only one symmetry class, where the pyroelectric coefficient is not fixed in a preferential crystallographic direction, but its orientation can change within a certain plane, here within the (010)-plane. The pyroelectric vector has the form $\boldsymbol{p}(T) = (p_1\ 0\ p_3)$. It can be obtained by measurements in two perpendicular directions within the (010)-plane. The absolute value and the direction of the pyroelectric vector simply result from the vector sum of the measured quantities. For an unambiguous assignment of the direction of the pyroelectric vector a measurement in a third direction has to be done. We have performed two measurements in orthogonal directions, but rotated against the first set by an angle of 21.5°. Thereby magnitude and direction variations of $\boldsymbol{p}$ are found, the sign being still undetermined.

In Fig. 4 the components of the pyroelectric vector, p_i, are given as a function of temperature. Figure 5 shows the absolute value of the pyroelectric vector as a function of temperature, and the direction is given by the angle ψ between the pyroelectric vector and the crystallographic [100]-axis. A slight maximum in the absolute value of the pyroelectric vector = pyroelectric coefficient, $|\boldsymbol{p}|$, at about 259 K is observed while the angle, characterizing the direction, decreases in the temperature range investigated from $\psi = 77°$ (100 K) to $\psi = 66°$ (320 K). This behaviour can be compared with lithium trihydrogen selenite [5] and lithium trideuteroselenite [6], where the direction of the spontaneous polarization varies by about 4° in the temperature range $180 \leqq T/\text{K} \leqq 360$. The dielectric ellipse and the direction of the pyroelectric coefficient for 200 K and 300 K are shown together with the calculated dipole moment $\boldsymbol{\mu}$ in Figure 6.

Electric Dipole Moment; Method of Increments

Using the method of bond increments for the calculation of the dipole moment, the charge separation between the ammonium ion and the $COO^{\ominus}$ group was treated in two ways. At first the part of the dipole moment resulting from $d(NH_4^{\oplus} \ldots COO^{\ominus})$ was calculated by assuming point charges at the sites of the nitrogen $N^{\oplus}$ and the

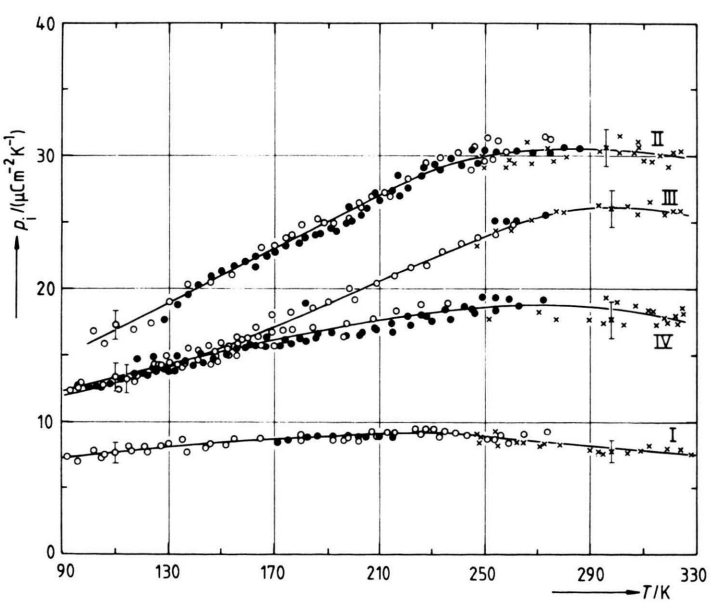

Fig. 4. Components of the pyroelectric vector, p_i, in different directions in the ac-plane characterized by θ_i. θ_i is defined as in the legend to Figure 3: I) $\theta_I = 142.1°$; II) $\theta_{II} = 52.1°$; III) $\theta_{III} = 30.6°$; and IV) $\theta_{IV} = 120.6°$. The full circles represent measurements done with increasing temperature, the open ones correspond to decreasing temperature. The data points obtained by use of the sinusoidal temperature oscillation method are labeled by crosses.

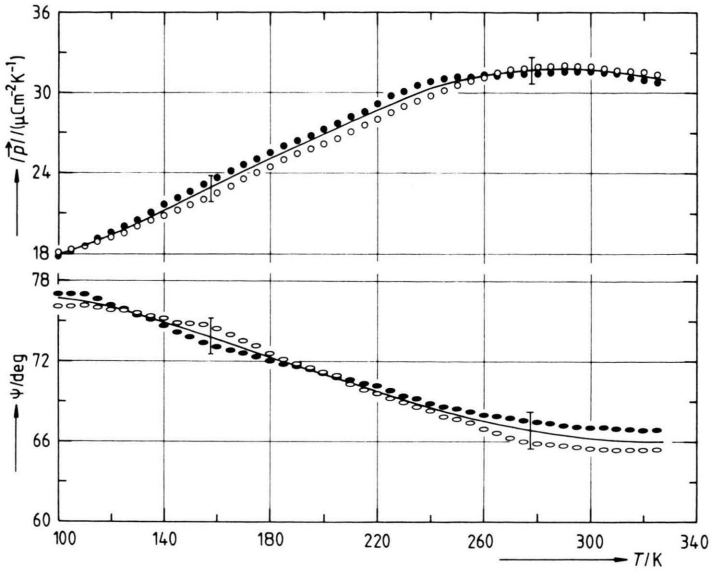

Fig. 5. Absolute value (upper part) of the pyroelectric vector, $|\boldsymbol{p}|$, and direction (lower part) of $\boldsymbol{p}$. ψ symbolizes the angle between $\boldsymbol{p}$ and the axis [100]. The full symbols are deduced from the curves I) and II) and the open symbols from the curves III) and IV) in Figure 4.

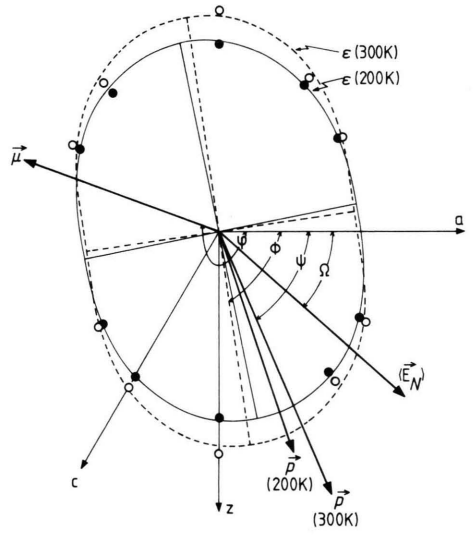

Fig. 6. Dielectric ellipse $\varepsilon(\theta)$ and pyroelectric vector $\pm \boldsymbol{p}$ (the sign of $\boldsymbol{p}$ is unknown) at $T = 200$ K and $T = 300$ K, together with the calculated dipole moment (INDO-SCEF) $\boldsymbol{\mu}$ and the electric field of the neighbouring molecules $\boldsymbol{E}_N$.

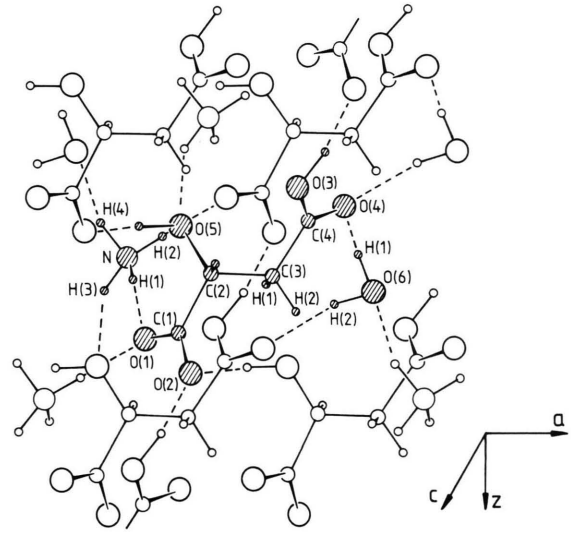

Fig. 7. Schematic display of the reference unit R (dashed) and the directions of the hydrogen bonds to the neighbours.

oxygen, $O(1)^{\ominus}$ (see Figure 7). This leads to the total dipole moment $\boldsymbol{\mu}_1$. In a second approach the negative point charge was located at the center of O(1) and O(2) ($\boldsymbol{\mu}_2$). From the symmetry of the space group it follows that, due to the glide plane, there is no component of $\boldsymbol{\mu}$ in the [010]-direction. The values found for $\boldsymbol{\mu}$ and for the angle φ between the dipole moment and the axis [100] are:

$$\boldsymbol{\mu}_1 = 30.2 \cdot 10^{-30}\,\mathrm{C\,m}, \quad \varphi_1 = 198°,$$

$$\boldsymbol{\mu}_2 = 40.5 \cdot 10^{-30}\,\mathrm{C\,m}, \quad \varphi_2 = 203°.$$

It is obvious that direction and value of the dipole moment are mainly fixed by the charge separation

between the $NH_4^{\oplus}$ and the $COO^{\ominus}$ group. The direction of $\boldsymbol{\mu}$ is defined $\ominus \rightarrow \oplus$.

Electric Dipole Moment and Net Charges from the SCEF-INDO Calculations

In the numerical INDO (SCEF) calculations we adopted the experimental structure parameters [1] for the unperturbed molecule $NH_4^{\oplus}({}^{\ominus}OOCCHOHCH_2COOH) \cdot H_2O$ in the vacuum and in the solid state. The formula unit R and the atomic numbering scheme are displayed in Figure 7. The external field has been build up in two types. In the first approach of approximation only eight external units have been employed. We have selected those neighbours N which are coupled to the reference system via hydrogen bonds. In the second calculation we constructed a spherical external field by means of 16 neighbouring molecules, i.e. an approximation beyond the nearest neighbour's scheme was used (Figure 2). It turned out that the additional external units had no significant influence on the calculated charge distribution, showing that modifications in the electronic structure of the title compound in the solid state are rather local effects caused by hydrogen bonded neighbours. Interactions beyond the nearest neighbour's are important only if lattice (Madelung) energies are calculated.

In Table 1 we have summarized the atomic net charges q_j of the title compound in the vacuum and in the external field created by 16 adjacent molecules. A comparison of the charge distribution in the vacuum and the solid shows large electronic reorganizations at those atomic sites that form hydrogen bonds to adjacent molecules. These redistributions are pronounced for O(2), O(3), O(4) as well as for the hydrogen atoms H(O3), H(1, N), H(2, N) and for the H atoms of the H_2O molecule. The charge separation between three atomic centers forming a hydrogen bridge is always enlarged. It leads to increasing electrostatic interactions that allow for a stabilization in the crystal.

Furthermore are given in Table 1 the dipole moment of the formula unit and the angle φ between the dipole moment and the axis [100]. Magnitude and direction of the dipole moment are comparable in both states, the vacuum and the solid. It is obvious, that the direction and magnitude is mainly fixed by the geometry of the molecule and the crystal lattice.

Table 1. Atomic net charges in one molecule (formula unit) of AMAL (see Figs. 2 and 7).

	Isolated molecule	Solid-state environment (16 molecules)
O(1)	− 0.81	− 0.83
O(2)	− 0.75	− 0.82
O(3)	− 0.49	− 0.65
O(4)	− 0.63	− 0.65
O(5)	− 0.54	− 0.60
O(6)	− 0.65	− 0.76
C(1)	0.71	0.74
C(2)	0.17	0.17
C(3)	− 0.30	− 0.34
C(4)	0.73	0.79
H(O3)	0.35	0.52
H(O5)	0.30	0.33
H(1, O6)	0.30	0.37
H(2, O6)	0.33	0.39
H(C2)	0.08	0.09
H(1, C3)	0.16	0.17
H(2, C3)	0.14	0.19
N	− 0.03	− 0.10
H(1, N)	0.25	0.29
H(2, N)	0.25	0.30
H(3, N)	0.21	0.19
H(4, N)	0.22	0.21
μ/C m	$44.7 \cdot 10^{-30}$	$44.1 \cdot 10^{-30}$
φ	200.0°	199.6°

Discussion

AMAL belongs to the group of substances with a pyroelectric coefficient, which can vary its direction with temperature within a symmetry plane. In this case the direction of $\boldsymbol{p}$ is an additional independent parameter in the calculation of $\boldsymbol{p} = f(T)$ compared to substances with a polar crystal axis.

The temperature dependence of the polarization $\boldsymbol{P}$ of AMAL is described by the model introduced in [7]. The crystal is treated as a dielectric medium, composed of dipoles with a permanent moment $\boldsymbol{\mu}$, with a dielectric constant ε, and a polarizability α. The internal field at the site of a dipole is built up by the Lorentz field $\boldsymbol{E}_L$ plus the electric field $\boldsymbol{E}_N$ of the neighbouring dipoles N, which are treated as point charges. The field $\boldsymbol{E}_N$ was calculated at the site of the reference unit R, using the atomic net charges determined by the SCEF approach, q_j, and the structure data from [1]

$$\boldsymbol{E}_N(x, y, z) = \frac{1}{4\pi\varepsilon_0} \sum_N \sum_j \frac{q_j \boldsymbol{r}_j}{|r_j|^3} \equiv \frac{1}{4\pi\varepsilon_0} \boldsymbol{S}_N(x, y, z), \tag{10}$$

with $\boldsymbol{r}_j$ = radius vector from atom j in the external molecule N to the reference unit R and $\boldsymbol{S}_N$ = abbreviation for the summation. The volume of the reference unit V_R was divided into volume elements ΔV of about $4 \cdot 10^{-32}\,m^{-3}$. For each volume element $\boldsymbol{E}_N(x, y, z)$ was calculated and in a further step $\boldsymbol{E}_N$ was averaged over V_R:

$$\langle \boldsymbol{E}_N \rangle = \frac{1}{V_R} \sum \boldsymbol{E}_N(x, y, z)\, \Delta V \equiv \frac{1}{4\pi\varepsilon_0} \langle \boldsymbol{S}_N \rangle. \quad (11)$$

By this method the mean electric field $\langle \boldsymbol{E}_N \rangle$ of the neighbouring molecules N averaged over the volume of the reference unit V_R is obtained. The direction of $\langle \boldsymbol{E}_N \rangle$ is characterized by $\Omega = \sphericalangle([100], \langle \boldsymbol{E}_N \rangle)$ (Figure 6).

Using the abovementioned physical parameters the polarization $\boldsymbol{P}$ of a crystal can be described [7] by

$$\boldsymbol{P} = \frac{N_A}{3\bar{V}} (\varepsilon_P + 2)\, |\boldsymbol{\mu}| \cos\delta + \frac{1}{4\pi} (\varepsilon_P - 1)\, |\langle \boldsymbol{S}_N \rangle| \cos\beta. \quad (12)$$

with $1/\bar{V} = \varrho/M$ = number of molecules per unit volume, ϱ = density = 1.50 Mg/m^3, M = molar mass = 169.13 g/mol, N_A = Avogadro number = $6.022 \cdot 10^{23}\,mol^{-1}$, $|\boldsymbol{\mu}|$ = dipole moment = $44.06 \cdot 10^{-30}$ C m, $|\langle \boldsymbol{S}_N \rangle| = 0.547\ C\,m^{-2}$, ε_P = dielectric constant in the direction of $\boldsymbol{P}$, δ = angle between $\boldsymbol{\mu}$ and $\boldsymbol{P}$, β = angle between $\langle \boldsymbol{E}_N \rangle$ and $\boldsymbol{P}$. Differentiation of (12) leads to an expression for the temperature dependence of the pyroelectric coefficient:

$$\begin{aligned} \boldsymbol{p} = \frac{d\boldsymbol{P}}{dT} = &- \frac{N_A}{3\bar{V}^2} (\varepsilon_P + 2)\, |\boldsymbol{\mu}| \cos\delta \frac{\partial \bar{V}}{\partial T} \\ &+ \frac{N_A}{3\bar{V}} (\varepsilon_P + 2)\, |\boldsymbol{\mu}| \frac{\partial \cos\delta}{\partial T} \\ &+ \frac{1}{4\pi} (\varepsilon_P - 1)\, |\langle \boldsymbol{S}_N \rangle| \frac{\partial \cos\beta}{\partial T} \\ &+ \left(\frac{N_A}{3\bar{V}} |\boldsymbol{\mu}| \cos\delta + \frac{1}{4\pi} |\langle \boldsymbol{S}_N \rangle| \cos\beta \right) \frac{\partial \varepsilon_P}{\partial T}. \end{aligned} \quad (13)$$

The first term can be set equal to zero as the temperature dependence of the volume can be neglected in the temperature range considered. ε_P and $\partial\varepsilon_P/\partial T$ are temperature dependent quantities, which can be extracted from the curves of Figure 3. Below $T = 200$ K extrapolated values have been used.

The direction of the polarization $\boldsymbol{P}$ which is necessary for the estimation of $\delta(T)$ and $\beta(T)$ can be approximated under the assumption that $d\boldsymbol{P}/dT = 0$ for $T \to 0$ K, e.g. the pyroelectric coefficient $\boldsymbol{p}$ and the polarization $\boldsymbol{P}$ are parallel at $T = 0$ K. An extrapolated value of the angle between the [100]-axis and $\boldsymbol{p}$ at $T = 0$ K from Fig. 5 is $\psi = 80°$. With this, $|\boldsymbol{P}|$ can be obtained from (12), $|\boldsymbol{P}| = 0.143\ C\,m^{-2}$. Using the direction and value of $\boldsymbol{P}_{T=0\,K}$ the variation of $\boldsymbol{P}(T)$ is described by

$$\boldsymbol{P}(T) = \int \boldsymbol{p}(T)\, dT. \quad (14)$$

The changes of δ and β with temperature are deduced directly from the angular variation of $\boldsymbol{P}(T)$, because the calculated dipole moment $\boldsymbol{\mu}$ and the electric field $\langle \boldsymbol{E}_N \rangle$ are assumed to be fixed over the whole temperature range.

Therefrom the temperature dependence of the pyroelectric coefficient can be obtained using (13) and introducing the following: The measured values for ε_P and $\partial\varepsilon_P/\partial T$, the values for $\cos\delta$ and $\cos\beta$ deduced as described above, and the calculated values for $\boldsymbol{\mu}$ and $\langle \boldsymbol{E}_N \rangle$. Introducing all constants and temperature-independent coefficients, (13) reduces to

$$\begin{aligned} \boldsymbol{p} = &\ 0.0784\,(\varepsilon_P + 2) \frac{\partial \cos\delta}{\partial T} + 0.0436\,(\varepsilon_P - 1) \frac{\partial \cos\beta}{\partial T} \\ &+ (0.0784 \cdot \cos\delta + 0.0436 \cos\beta) \frac{\partial \varepsilon_P}{\partial T} \\ = &\ \boldsymbol{p}(\mathrm{I}) + \boldsymbol{p}(\mathrm{II}) + \boldsymbol{p}(\mathrm{III}). \end{aligned} \quad (15)$$

In Table 2 the values for ε_P and $\partial\varepsilon_P/\partial T$ are given for selected temperatures, together with the $\cos\delta$ and $\cos\beta$. Additionally the data for $|\boldsymbol{p}|$(calc) = $|\boldsymbol{p}|(1)$ and $|\boldsymbol{p}|$(exp) are listed. The resulting curve $|\boldsymbol{p}|(1) = |\sum \boldsymbol{p}(1, i)|$ with i = I, II, III in Fig. 8 follows the trend of the measured one, $|\boldsymbol{p}|$(exp), as there is an increase in the temperature range $100 \leqq T/K \leqq 280$. But the maximum in $|\boldsymbol{p}|$(exp) is not found and the increase of $|\boldsymbol{p}|$ with T is heavily overestimated, reaching a value of the pyroelectric coefficient which is three times as large as $|\boldsymbol{p}|$(exp). In Fig. 8 the components $|\boldsymbol{p}|(1, \mathrm{I})$ to $|\boldsymbol{p}|(1, \mathrm{III})$ of $|\boldsymbol{p}|(1)$ corresponding to the three terms in (15) are given, too. $\boldsymbol{p}(1, \mathrm{II})$ has the opposite sign of $\boldsymbol{p}(1, \mathrm{I})$ and $\boldsymbol{p}(1, \mathrm{III})$. It is easily seen that the main part of the temperature dependence of $\boldsymbol{p}(1)$ is due to $\boldsymbol{p}(1, \mathrm{III})$, e.g. the temperature dependence of the dielectric constant ε_P.

Table 2. Compilation of the different physical parameters either measured or calculated, which have been used in the calculation of the pyroelectric coefficient $|\boldsymbol{p}|$ (see text). For comparison the calculated values $|\boldsymbol{p}|(1) - |\boldsymbol{p}|(3)$ are given together with $|\boldsymbol{p}|$ (exp).

T/K	120	160	200	240	280	320
ε_P	7.20	7.31	7.46	7.70	8.14	8.70
$\partial\varepsilon_P/\partial T \cdot 10^3$	2.25	3.25	4.50	8.30	12.10	14.70
$\cos\delta$	− 0.4942	− 0.4947	− 0.4958	− 0.4970	− 0.4986	− 0.5005
$\partial\cos\delta/\partial T \cdot 10^5$	− 1.0	− 1.4	− 2.5	− 3.5	− 4.4	− 4.75
$\cos\beta$	0.7850	0.7854	0.7861	0.7869	0.7881	0.7894
$\partial\cos\beta/\partial T \cdot 10^5$	1.12	1.37	1.87	2.5	3.12	3.25
$\|\boldsymbol{p}\|(1)/(\mu C\,m^{-2}\,K^{-1})$	14.8	22.7	34.5	58.3	82.1	98.0
$\|\boldsymbol{p}\|(2)/(\mu C\,m^{-2}\,K^{-1})$	6.8	10.2	18.2	29.1	39.7	46.6
$\|\boldsymbol{p}\|(3)/(\mu C\,m^{-2}\,K^{-1})$	2.7	7.0	13.4	18.3	23.5	26.2
$\|\boldsymbol{p}\|$ (exp)/$(\mu C\,m^{-2}\,K^{-1})$	19.3	23.1	26.6	30.4	31.7	31.2

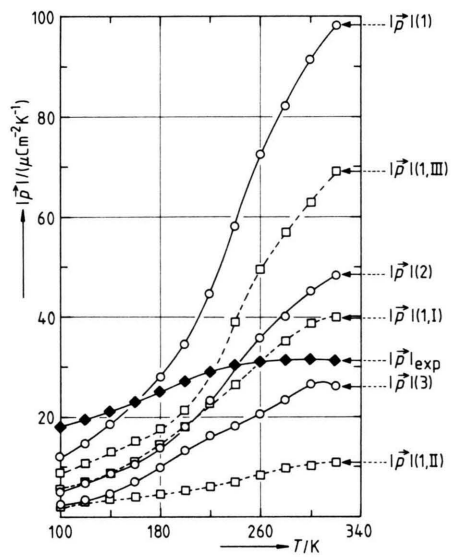

Fig. 8. Calculated pyroelectric coefficients $|\boldsymbol{p}|(1) - |\boldsymbol{p}|(3)$, together with the measured one $|\boldsymbol{p}|$ (exp).

From the values used in the calculations, the dipole moment $\boldsymbol{\mu}$ and the field $|\langle \boldsymbol{E}_N \rangle|$ arising from the neighbouring molecules N at the site of the reference unit R introduce the largest uncertainty. It is known that semiempirical LCAO-calculations describe dipole moments not better than to about 20% [13]. For the electric field $|\langle \boldsymbol{E}_N \rangle|$, which arises from the semiempirically calculated charge distribution, unfortunately the same is true. Therefore $|\langle \boldsymbol{E}_N \rangle|$ was varied within the limits of error to test the dependency of $\boldsymbol{p}(T)$.

Using values of $1.1 \cdot |\langle \boldsymbol{E}_N \rangle|$ and $1.15 \cdot |\langle \boldsymbol{E}_N \rangle|$ in the calculations of the pyroelectric coefficient, curves $|\boldsymbol{p}|(2)$ and $|\boldsymbol{p}|(3)$ in Fig. 8 are obtained. Obviously curve $|\boldsymbol{p}|(2)$ is in better accordance with $|\boldsymbol{p}|$ (exp), while curve $|\boldsymbol{p}|(3)$, e.g. the curve calculated with a deviation of + 15% in $|\langle \boldsymbol{E}_N \rangle|$, shows already a smaller value. The curvature of $|\boldsymbol{p}|$ (exp) is represented best by the calculated curve $|\boldsymbol{p}|(3)$ while the magnitude is in the order of $|\boldsymbol{p}|(2)$.

The used variation of $|\langle \boldsymbol{E}_N \rangle|$ causes a drastic change of the value of the third term in (15), while the first and second terms remain almost unchanged. This change is due to the difference of the dipole field and the internal field in the third term. $(a \cdot \cos\delta + b \cdot \cos\beta)$ is practically independent of T and therefore acts as a scaling factor for the influence of the temperature dependence of the dielectric constant upon the pyroelectric coefficient. The employed model shows a sensitive response upon small disturbances. Nevertheless the measured pyroelectric coefficient can be represented within the limits of error of the used parameters. It is noted that only physical relevant values are employed in the calculations and no free parameters fitted to the experimental curve have been introduced into it.

Acknowledgement

We are grateful to the Stiftung Volkswagenwerk for support of this work.

[1] J. F. J. van Loock, M. van Hooste, and A. T. H. Lenstra, Bull. Sco. Chim. Belg. **90,** 155 (1981).
[2] W. Versichel, W. van de Mieroop, and A. T. H. Lenstra, Acta Crystallogr. **B 34,** 2643 (1978).
[3] P. Seiler, B. Martinoni, and J. D. Dunitz, Nature **309,** 435 (1984).
[4] K. Betzler, H. Hesse, and P. Loose, J. Mol. Struct. **47,** 393 (1978).
[5] D. Berlincourt, W. R. Cook, and M. E. Rander, Acta Crystallogr. **16,** 163 (1963).
[6] L. A. Shuvalov, V. W. Anisimova, N. R. Ivanov, and I. A. Velichko, Sov. Phys. Crystallogr. **17,** 1096 (1973).
[7] S. Fleck and Al. Weiss, Z. Naturforsch. **41a,** 1289 (1986).
[8] T. Asaji and Al. Weiss, Z. Naturforsch. **40a,** 567 (1985).
[9] C. Bèguin and T. Gaumann, Helv. Chim. Acta **41,** 1376 (1958).
[10] C. P. Smyth, Dielectric Behaviour and Structure, McGraw-Hill, New York 1955.
[11] Landolt-Börnstein II/6, Molecular Constants, Springer-Verlag, Berlin 1974; II/14, ibid. 1982.
[12] J. A. Pople and D. L. Beveridge, Approximate Molecular Orbital Theory, McGraw-Hill, New York 1970.
[13] M. C. Böhm and R. Gleiter, Theor. Chim. Acta **59,** 127, 153 (1981).
[14] M. C. Böhm, Physica **124 B,** 327 (1984).
[15] M. C. Böhm, Phys. stat. sol. (b) **121,** 255 (1984).
[16] J. N. Murrell, M. Randić, and O. R. Williams, Proc. Roy. Soc. (London) **A 284,** 566 (1965).
[17] E. V. Condon and C. H. Shortley, The Theory of Atomic Spectra, Cambridge University Press, Cambridge 1970.
[18] R. S. Mulliken, J. Chem. Phys. **23,** 1833 (1955).
[19] R. S. Mulliken, J. Chim. Phys. **46,** 497, 675 (1949).
[20] J. F. Nye, Physical Properties of Crystals, Clarendon Press, Oxford 1957.